

CYANAMIDE (NH_2CN) IN INTERSTELLAR MEDIUM: POTENTIAL SPECTRAL LINES

M.K.SHARMA

Received 30 April 2019

Accepted 23 December 2020

Cyanamide (NH_2CN) has pyramidal equilibrium structure with two substates, denoted by 0^+ and 0^- . For each state of NH_2CN , knowing rotational and centrifugal distortion constants in conjunction with electric dipole moment, energies for rotational levels and the probabilities for radiative transitions between the levels are calculated. The radiative transition probabilities in conjunction with scaled values for rate coefficients for collisional transitions between the levels are used in the Large Velocity Gradient analysis for each substate. For each substate, we have found anomalous absorption in three doublets at high temperature and weak MASER action at low temperature. We have also found emission feature in nine transitions in each substate. These transitions, along with the observed ones, may play important role for identification of NH_2CN in a cosmic object.

Keywords: *molecules: NH_2CN ; Einstein A-coefficients; radiative transfer*

1. *Introduction.* Containing two atoms of nitrogen, cyanamide is one of the rare interstellar molecules. It is considered relevant for prebiotic chemistry, as in the liquid water, it may convert into urea which is important in the biological processes [1]. It is found to have pyramidal equilibrium structure with two substates, denoted by 0^+ and 0^- . Spectrum analysis of cyanamide is carried out from time to time [2-9]. We have considered spectroscopic data of Coutens et al. [9]. For both the substates, rotational and centrifugal distortion constants reported by Coutens et al. [9] are used in the present investigation and are reported in Table 1. The substates 0^+ and 0^- have electric dipole moment $\mu_a = 4.25 \pm 0.02\text{D}$ and $\mu_a = 4.24 \pm 0.02\text{D}$, respectively [3]. Because of two hydrogen atoms, each substate has ortho and para species. In the 0^+ substate, ortho specie is described by even value of k_a , whereas the case is reverse for the 0^- substate. First detection of cyanamide towards solar-type protostars, IRAS 16293B and towards IRAS2A are reported by Coutens et al. [8]. This molecule has also been detected in other galaxies, such as NGC 253 and M82 [10,11], in the massive star-forming regions Sgr B2 [12,13], in solar-type protostar IRAS 162932422 B [9] and in high-mass proto-star IRAS 20126+410 [14].

In the ground vibrational state, they [8] have found $17_{0,17}-16_{0,16}$, $17_{2,15}-16_{2,14}$, $18_{1,18}-17_{1,17}$, $18_{2,16}-17_{2,15}$, $18_{3,16}-17_{3,15}$, $18_{3,15}-17_{3,14}$, and $18_{1,17}-17_{1,16}$ transitions in IRAS

Table 1

ROTATIONAL AND CENTRIFUGAL DISTORTION CONSTANTS
OF NH₂CN IN MHz

Constant	0 ⁺ substate	0 ⁻ substate
<i>A</i>	312142.025	304454.083
<i>B</i>	10129.75679	10112.65371
<i>C</i>	9866.659953	9865.923593
<i>D_J</i>	$3.741178 \cdot 10^{-3}$	$3.7782 \cdot 10^{-3}$
<i>D_{JK}</i>	$396.199 \cdot 10^{-3}$	$359.211 \cdot 10^{-3}$
<i>D_K</i>	44.1278	27.9564
<i>d₁</i>	$-140.8332 \cdot 10^{-6}$	$-119.7066 \cdot 10^{-6}$
<i>d₂</i>	$-32.5952 \cdot 10^{-6}$	$-21.9978 \cdot 10^{-6}$
<i>H_J</i>	$-1.031 \cdot 10^{-9}$	$-0.621 \cdot 10^{-9}$
<i>H_{JK}</i>	$1.3677 \cdot 10^{-6}$	$0.7919 \cdot 10^{-6}$
<i>H_{KJ}</i>	$-338.05 \cdot 10^{-6}$	$-190.77 \cdot 10^{-6}$
<i>H_K</i>	$17.213 \cdot 10^{-3}$	$4.307 \cdot 10^{-3}$
<i>L_{JK}</i>	$12.47 \cdot 10^{-9}$	$12.47 \cdot 10^{-9}$
<i>L_{KKJ}</i>	$-4.034 \cdot 10^{-6}$	$-3.328 \cdot 10^{-6}$
<i>L_K</i>	$21.33 \cdot 10^{-6}$	$10.69 \cdot 10^{-6}$

16293 B, and 12_{1,11}-11_{1,10} and 16_{1,16}-15_{1,15} transitions in IRAS2A. Most of the transitions in are both the substates. The comparison of frequencies shows that all these nine transitions belong to the 0⁺ substate.

Using the spectroscopic data (rotational and centrifugal distortion constants, and electric dipole moment), we have calculated energies of 120 rotational levels of each specie in each substate and the radiative transition probabilities (Einstein *A* and *B* coefficients) for radiative transitions between the levels by using the computer code ASROT [15]. The radiative transition probabilities in conjunction with scaled values of collisional rate coefficients are used for solving a set of 120 statistical equilibrium equations coupled with the equations of radiative transfer. Out of a large number of lines, we have considered the strongest emission and absorption lines. In each substate, three doublets, 1₁₀-1₁₁, 2₁₁-2₁₂, 3₁₂-3₁₃ are found to show anomalous absorption at high temperature and weak MASER action at low temperature. In each substate, nine transitions, 4₁₄-3₁₃, 5₁₅-4₁₄, 6₁₆-5₁₅, 3₀₃-2₀₂, 4₀₄-3₀₃, 5₀₅-4₀₄, 7₀₇-6₀₆, 8₀₈-7₀₇, 9₀₉-8₀₈ are found to show emission feature. The intensities of observed lines are found weaker than the lines discussed here. These lines, along with the observed ones, may play important role in the detection of cyanamide in a cosmic object.

2. *Model.* The model used here is the same as discussed by Sharma et al. [16-20]. In the Large Velocity Gradient (LVG) analysis, a set of statistical

equilibrium equations coupled with the equations of radiative transfer is written as the following.

$$n_i \sum_{\substack{j=1 \\ j \neq i}}^{120} P_{ij} = \sum_{\substack{j=1 \\ j \neq i}}^{120} n_j P_{ji} \quad i = 1, 2, \dots, 120 \quad (1)$$

where n denotes the population density of energy level and the parameter P is as the following.

(i) For a radiatively allowed transition

$$P_{ij} = \begin{cases} (A_{ij} + B_{ij} I_{\nu, bg}) \beta_{ij} + n_{H_2} C_{ij} & i > j \\ B_{ij} I_{\nu, bg} \beta_{ij} + n_{H_2} C_{ij} & i < j \end{cases}$$

(ii) For a radiatively forbidden transition

$$P_{ij} = n_{H_2} C_{ij} .$$

Here, A and B are the Einstein coefficients, C the rate coefficient for collisional transition and n_{H_2} the density of molecular hydrogen. The escape probability β for the transition is

$$\beta_{lu} = \beta_{ul} = \frac{1 - \exp(-\tau_\nu)}{\tau_\nu},$$

where optical depth τ_ν is expressed as

$$\tau_\nu = \frac{hc}{4\pi(dv_r/dr)} [B_{lu} n_l - B_{ul} n_u],$$

where (dv_r/dr) denotes the velocity gradient in the region. This is non-linear set of equations.

The external radiation field impinging on the volume element, generating the lines, is the cosmic microwave background (CMB) only, which corresponds to the background temperature $T_{bg} = 2.73$ K. The parameter γ is expressed as $\gamma = n_{mol}/(dv_r/dr)$. Here, n_{mol} is the density of the species of cyanamide and (dv_r/dr) the velocity gradient in the object. Equation (1) is a set of homogeneous equations which does not have unique solution. In order to make the set of equations inhomogeneous, the last statistical equilibrium equation is replaced by the following equation, showing conservation.

$$\sum_{i=1}^{120} n_i = n_{mol} .$$

Using the values of radiative and collisional transition probabilities, each set of non-linear equations is solved through iterative procedure where the initial population densities of levels are taken as the thermal populations, corresponding to the kinetic temperature.

2.1. *Radiative transitions in cyanamide.* In each substate, the electric dipole moment is along a -axis of inertia. The radiative transitions are governed by the selection rules:

$$J: \Delta J = 0, \pm 1$$

$$k_a, k_c: \text{ even, even} \leftrightarrow \text{ even, odd}$$

$$k_a, k_c: \text{ odd, even} \leftrightarrow \text{ odd, odd}.$$

For 120 rotational levels, for each specie in each substate, the 0^+ substate has 309 ortho and 310 para transitions whereas in the 0^- substate, there are 308 ortho and 309 para transitions. For the given values of rotational and centrifugal distortion constants, and electric dipole moment, we have calculated energies of 120 rotational levels and line strengths for radiative transitions between the levels with the help of the software ASROT [15].

For a radiative transition from upper level u to lower level l , the line-strength S_{ul} ($=S_{lu}$) is related to the Einstein A -coefficient, A_{ul} , as

$$A_{ul} = \frac{64\pi^4 \nu_{ul}^3 \mu_1^2}{3 g_u h c^3} S_{ul},$$

where g_u ($=2J_u + 1$) is the statistical weight of upper level with rotational quantum number J_u , μ_1 is component of electric dipole moment and ν_{ul} the frequency of transition. The Einstein A and B coefficients are related through the relations:

$$A_{ul} = \frac{8\pi h \nu^3}{c^3} B_{ul} \quad \text{and} \quad B_{lu} = \frac{g_u}{g_l} B_{ul},$$

where g_l denotes the statistical weights for the lower level.

2.2. *Collisional transitions.* Though the collisional transitions, contrary to the radiative transitions, between the rotational levels do not follow any selection rules, the calculation of collisional rate coefficients for the transitions is a difficult task [21-23]. The collisional rate coefficients for cyanamide are not available, therefore, they are estimated following the procedure discussed by Sharma et al. [16,17,19,20,24].

$$C(J'_{k'_a, k'_c} \rightarrow J_{k_a, k_c}) = \frac{10^{-11}}{2J'+1} \sqrt{\frac{T}{30}}.$$

This expression is equivalent to the cross section times the relative velocity of collision partner, which is generally taken as the molecular hydrogen H_2 , whose abundance is the largest in a molecular region. These collisional rate coefficients are such that they do not generate any anomalous phenomenon from their own.

3. *Results and discussion.* In order to consider a large number of cosmic objects, where the cyanamide may be found, the calculations are done for wide

ranges of physical quantities. The molecular hydrogen density n_{H_2} is taken from 10^2 to 10^6 cm^{-3} ; the kinetic temperatures T are 20, 40, 60, 80, 100 K. However, in figures we have given the values for 40 and 100 K. Two values of $\gamma [= n_{\text{mol}} / (d v_r / dr)]$ are taken as 10^{-5} and $10^{-6} \text{ cm}^{-3} (\text{km/s})^{-1} \text{ pc}$. Here, n_{mol} is the density of the species of NH_2CN and $(d v_r / dr)$ the velocity-gradient in the region.

In Fig.1, we have plotted brightness temperature versus hydrogen density for two temperatures, 40 and 100 K (written on the top) for six para transitions (written on the left) in 0^+ substate. Fig.2, is the same as Fig.1, but for six ortho transitions in 0^+ substate. Fig.3 and 4 are for ortho and para transitions, respectively, in the 0^- substate. The kinks in the plots are due to numerical instabilities. Interesting to note that Fig.1 and 3 are very similar whereas Fig.2 and 4 are very similar.

Three doublets, $1_{10}-1_{11}$, $2_{11}-2_{12}$, $3_{12}-3_{13}$ in each substate are found to show anomalous absorption at high temperature and weak MASER action at low temperature. The transition $1_{10}-1_{11}$, in particular, may be utilized as a probe for the search of molecule. In each substate, nine transitions, $4_{14}-3_{13}$, $5_{15}-4_{14}$, $6_{16}-5_{15}$,

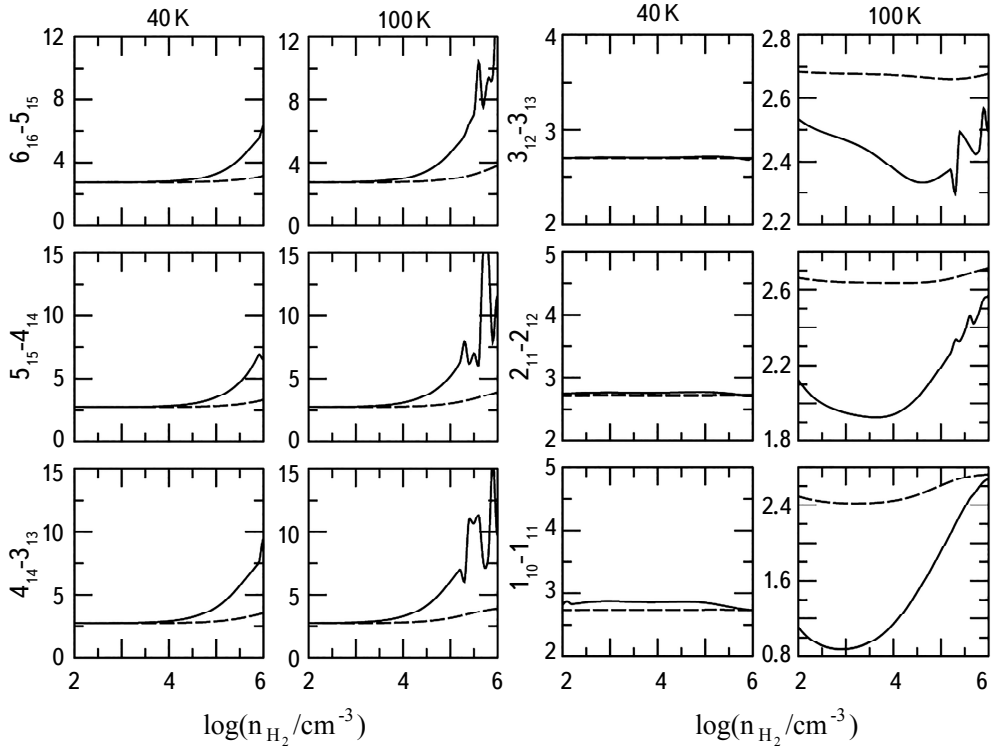


Fig.1. Variation of brightness temperatures T_B (K) versus molecular hydrogen density n_{H_2} for kinetic temperatures 40 and 100 K (written at the top) for six para transitions (written on the left) in 0^+ substate of NH_2CN . Solid line is for $\gamma = 10^{-5} \text{ cm}^{-3} (\text{km/s})^{-1} \text{ pc}$, and dotted line for $\gamma = 10^{-6} \text{ cm}^{-3} (\text{km/s})^{-1} \text{ pc}$.

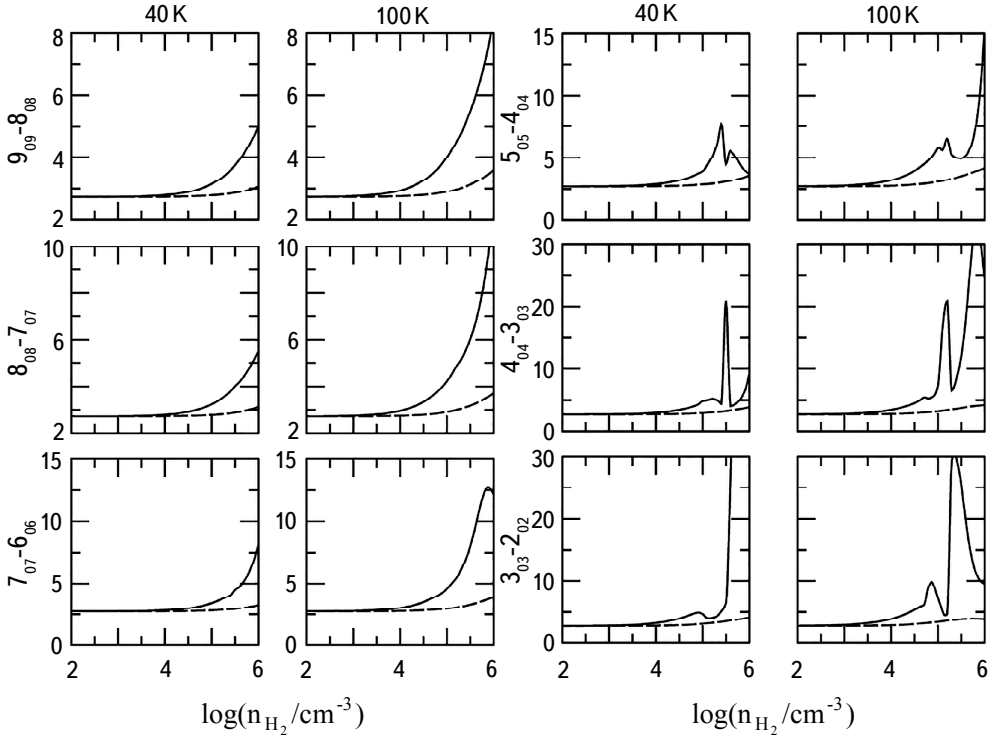


Fig.2. Same as for Fig.1, but for six ortho transitions (written on the left) in 0^+ substate of NH_2CN .

Table 2

FREQUENCY, EINSTEIN A-COEFFICIENT, ENERGY OF UPPER LEVEL, RADIATIVE LIFE-TIMES OF UPPER AND LOWER LEVELS FOR TRANSITIONS IN 0^+ SUBSTATE OF NH_2CN

Transition	ν (MHz)	A_{ul} (s^{-1})	E_u (cm^{-1})	t_u (s)	t_l (s)
$1_{10}-1_{11}$	263.096	$1.914 \cdot 10^{-12}$	10.7409	$5.22 \cdot 10^{11}$	∞
$2_{11}-2_{12}$	789.280	$1.723 \cdot 10^{-11}$	12.0827	$2.43 \cdot 10^5$	$2.53 \cdot 10^5$
$3_{12}-3_{13}$	1578.540	$6.891 \cdot 10^{-11}$	14.0954	$5.67 \cdot 10^4$	$5.90 \cdot 10^4$
$4_{14}-3_{13}$	79455.036	$4.394 \cdot 10^{-5}$	16.6913	$2.28 \cdot 10^4$	$5.90 \cdot 10^4$
$5_{15}-4_{14}$	99317.825	$8.988 \cdot 10^{-5}$	20.0019	$1.11 \cdot 10^4$	$2.28 \cdot 10^4$
$6_{16}-5_{15}$	119179.967	$1.597 \cdot 10^{-4}$	23.9745	$6.26 \cdot 10^3$	$1.11 \cdot 10^4$
$3_{03}-2_{02}$	59988.159	$1.945 \cdot 10^{-5}$	3.9992	$5.14 \cdot 10^4$	$1.86 \cdot 10^5$
$4_{04}-3_{03}$	79982.990	$4.781 \cdot 10^{-5}$	6.6652	$2.09 \cdot 10^4$	$5.14 \cdot 10^4$
$5_{05}-4_{04}$	99976.775	$9.550 \cdot 10^{-5}$	9.9979	$1.05 \cdot 10^4$	$2.09 \cdot 10^4$
$7_{07}-6_{06}$	139960.159	$2.690 \cdot 10^{-4}$	18.6622	$3.72 \cdot 10^3$	$5.97 \cdot 10^3$
$8_{08}-7_{07}$	159960.235	$4.049 \cdot 10^{-4}$	23.9939	$2.47 \cdot 10^3$	$3.72 \cdot 10^3$
$9_{09}-8_{08}$	179936.219	$5.802 \cdot 10^{-4}$	29.9917	$1.72 \cdot 10^3$	$2.47 \cdot 10^3$

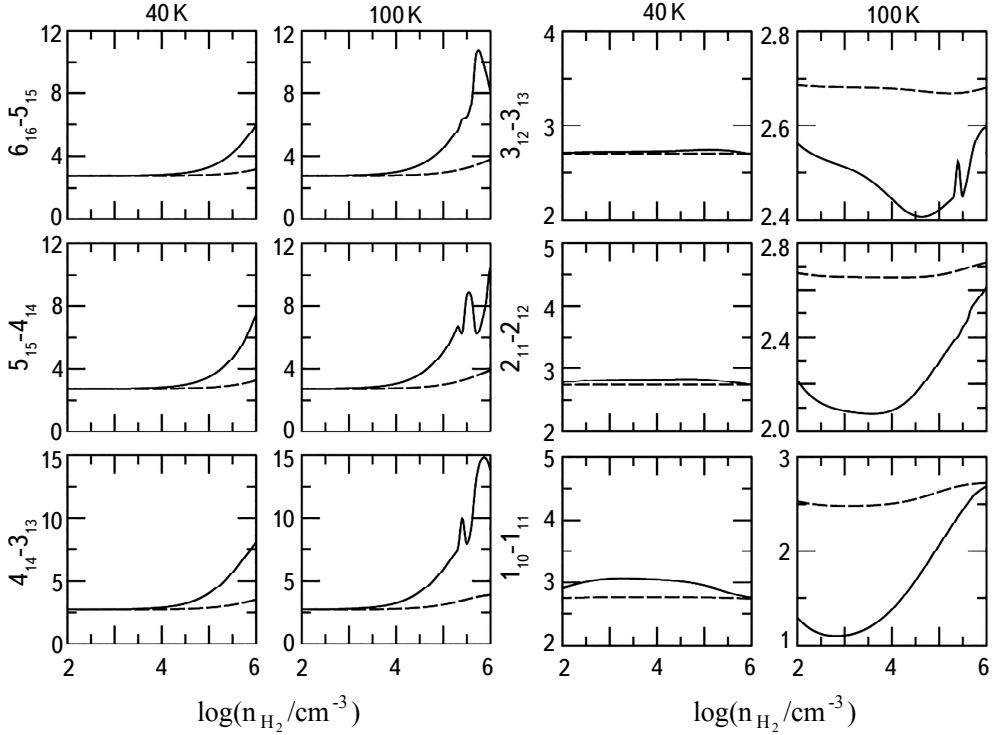

 Fig.3. Same as for Fig.1, but for six ortho transitions (written on the left) in 0^- substate of NH_2CN .

Table 3

FREQUENCY, EINSTEIN A-COEFFICIENT, ENERGY OF UPPER
 LEVEL, RADIATIVE LIFE-TIMES OF UPPER AND LOWER LEVELS
 FOR TRANSITIONS IN 0^- SUBSTATE OF NH_2CN

Transition	ν (MHz)	A_{ul} (s^{-1})	E_u (cm^{-1})	t_u (s)	t_l (s)
$1_{10}-1_{11}$	246.729	$1.571 \cdot 10^{-12}$	10.4846	$6.37 \cdot 10^{11}$	∞
$2_{11}-2_{12}$	740.182	$1.414 \cdot 10^{-11}$	11.8247	$2.45 \cdot 10^5$	$2.54 \cdot 10^5$
$3_{12}-3_{13}$	1480.346	$5.657 \cdot 10^{-11}$	13.8348	$5.72 \cdot 10^4$	$5.93 \cdot 10^4$
$4_{14}-3_{13}$	79416.727	$4.367 \cdot 10^{-5}$	16.4327	$2.29 \cdot 10^4$	$5.93 \cdot 10^4$
$5_{15}-4_{14}$	99269.960	$8.933 \cdot 10^{-5}$	19.7417	$1.12 \cdot 10^4$	$2.29 \cdot 10^4$
$6_{16}-5_{15}$	119122.561	$1.587 \cdot 10^{-4}$	23.7124	$6.30 \cdot 10^3$	$1.12 \cdot 10^4$
$3_{03}-2_{02}$	59934.703	$1.931 \cdot 10^{-5}$	3.9957	$5.18 \cdot 10^4$	$1.87 \cdot 10^5$
$4_{04}-3_{03}$	79911.791	$4.746 \cdot 10^{-5}$	6.6584	$2.11 \cdot 10^4$	$5.18 \cdot 10^4$
$5_{05}-4_{04}$	99887.896	$9.480 \cdot 10^{-5}$	9.9890	$1.05 \cdot 10^4$	$2.11 \cdot 10^4$
$7_{07}-6_{06}$	139836.173	$2.670 \cdot 10^{-4}$	18.6456	$3.75 \cdot 10^3$	$6.01 \cdot 10^3$
$8_{08}-7_{07}$	159807.855	$4.019 \cdot 10^{-4}$	23.9726	$2.49 \cdot 10^3$	$3.75 \cdot 10^3$
$9_{09}-8_{08}$	179777.572	$5.759 \cdot 10^{-4}$	29.9651	$1.74 \cdot 10^3$	$2.49 \cdot 10^3$

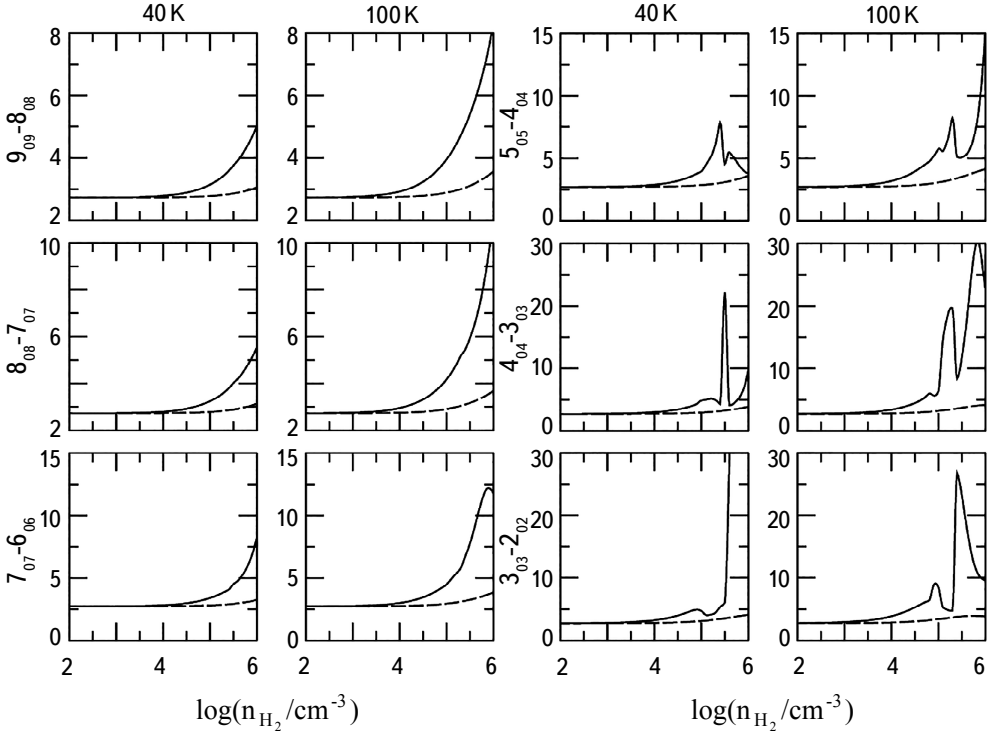


Fig.4. Same as for Fig.1, but for six para transitions (written on the left) in 0^- substate of NH_2CN .

$3_{03}-2_{02}$, $4_{04}-3_{03}$, $5_{05}-4_{04}$, $7_{07}-6_{06}$, $8_{08}-7_{07}$, $9_{09}-8_{08}$ are found to show emission feature. The intensity of a transition is found to increase with the increase of density and kinetic temperature. Parameters for these transitions are given in Tables 2 and 3 for 0^+ and 0^- substate, respectively. For all 24 transitions, the life time of lower level is found larger than that of the upper level. Still finding MASER action is interesting feature.

All nine observed lines, $17_{0.17}-16_{0.16}$, $17_{2.15}-16_{2.14}$, $18_{1.18}-17_{1.17}$, $18_{2.16}-17_{2.15}$, $18_{3.16}-17_{3.15}$, $18_{3.15}-17_{3.14}$, $18_{1.17}-17_{1.16}$, $12_{1.11}-11_{1.10}$ and $16_{1.16}-15_{1.15}$ in 0^+ substate are found to have weaker intensity as compared to those discussed above. Besides the observed lines, the lines discussed here may play important role in the detection of cyanamide in a cosmic object.

4. Conclusions. The LVG analysis carried out for 0^+ and 0^- substates of NH_2CN has found 12 additional transitions, $1_{10}-1_{11}$, $2_{11}-2_{12}$, $3_{12}-3_{13}$, $5_{15}-4_{14}$, $6_{16}-5_{15}$, $3_{03}-2_{02}$, $4_{04}-3_{03}$, $5_{05}-4_{04}$, $7_{07}-6_{06}$, $8_{08}-7_{07}$, $9_{09}-8_{08}$ transitions, for each state, which may help in the identification of cyanamide in a cosmic object.

Acknowledgements. The author is grateful to learned Reviewer for encouraging and constructive comments. He is also grateful to Hon'ble Dr. Ashok

K. Chauhan, Founder President, and Hon'ble Dr. Atul Chauhan, Chancellor, Prof. Dr. Balvinder Shukla, Vice Chancellor, Amity University for valuable support and encouragements. He is thankful to the SERB, Department of Science & Technology, New Delhi for awarding the NPDF.

Amity Center for Astronomy & Astrophysics, Amity Institute of Applied Sciences, Amity University, Noida 201313, India
e-mail: mohitkumarsharma32@yahoo.in mksharma4@amity.edu

ЦИАНАМИД (NH_2CN) В МЕЖЗВЕЗДНОЙ СРЕДЕ: ВОЗМОЖНЫЕ СПЕКТРАЛЬНЫЕ ЛИНИИ

М.К. ШАРМА

Цианамид (NH_2CN) имеет пирамидальную структуру равновесия с двумя подсостояниями, обозначенными 0^+ и 0^- . Для каждого состояния NH_2CN , зная константы вращательного и центробежного дисторсий в сочетании с электрическим дипольным моментом, вычислены энергии вращательных уровней и вероятности радиационных переходов между уровнями. Используя вероятности радиационных переходов в сочетании с масштабированными значениями коэффициентов скорости для столкновительных переходов между уровнями, выполнен LVG анализ для каждого подсостояния. Для каждого подсостояния мы обнаружили аномальное поглощение в трех дублетах при высокой температуре и слабый мазерный эффект при низкой температуре.

Мы также обнаружили особенности излучения в девяти переходах в каждом подсостоянии. Эти переходы, наряду с наблюдаемыми, могут играть важную роль для идентификации NH_2CN в астрофизических объектах.

Ключевые слова *ISM: молекулы, NH_2CN : A-коэффициенты Эйнштейна: перенос излучения*

REFERENCES

1. *M.L.Kilpatrick*, J. Am. Chem. Soc., **69**, 40, 1947.
2. *J.K.Tyler, J.Sheridan, C.C.Costain*, J. Mol. Spectrosc., **43**, 248, 1972.
3. *R.D.Brown, P.D.Godfrey, B.K.Nomer*, J. Mol. Spectrosc., **114**, 257, 1985.
4. *W.G.Read, E.A.Cohen, H.M.Pickett*, Mol. Spect., **115**, 316, 1986.
5. *M.Birk, M.Winnewisser, E.A.Cohen*, J. Mol. Spectrosc., **159**, 69, 1993.
6. *A.Krasnicki, Z.Kisiel, W.Jabs et al.*, J. Mol. Spectrosc., **267**, 144, 2011.
7. *Z.Kisiel, A.Krasnicki, W.Jabs et al.*, J. Phys. Chem. A, **117**, 9889, 2013.
8. *A.Coutens, E.R.Willis, R.T.Garrod et al.*, Astron. Astrophys., **612**, A107, 2018.
9. *A.Coutens, O.Zakharenko, F.Lewen et al.*, Astron. Astrophys., **623**, A93, 2019.
10. *S.Martin, R.Mauersberger, J.Martin-Pintado et al.*, Astrophys. J. Suppl., **164**, 450, 2006.
11. *R.Aladro, S.Martin, J.Martin-Pintado et al.*, Astron. Astrophys., **535**, A84, 2011.
12. *B.E.Turner, H.S.Liszt, N.Kaifu et al.*, Astrophys. J., **201**, L149, 1975.
13. *G.J.White, M.Araki, J.S.Greaves et al.*, Astron. Astrophys., **407**, 589, 2003.
14. *A.Palau, C.Walsh, A.Snchez-Monge et al.*, Mon. Not. Roy. Astron. Soc., **467**, 2723, 2017.
15. *Z.Kisiel, J.Demaison et al.*, (Eds.), Spectroscopy from Space, Kluwer, Dordrecht, 91, 2001.
16. *M.K.Sharma, M.Sharma, S.Chandra*, Astrophys. Space Sci., **362**, 168, 2017.
17. *M.K.Sharma, M.Sharma, S.Chandra*, Astrophys. Space Sci., **363**, 94, 2018a.
18. *M.K.Sharma*, J. Mol. Spectrosc., **15**, 1, 2019.
19. *M.K.Sharma, M.Sharma, S.Chandra*, Mol. Astrophys., **12**, 20, 2018b.
20. *M.K.Sharma*, Astron. Astrophys., **40**, 10, 2019.
21. *M.Sharma, M.K.Sharma, U.P.Verma et al.*, Adv. Space Res., **54**, 252, 2014a.
22. *M.K.Sharma, M.Sharma, U.P.Verma et al.*, Adv. Space Res., **54**, 1963, 2014b.
23. *M.K.Sharma, M.Sharma, U.P.Verma et al.*, Adv. Space Res., **55**, 434, 2015.
24. *M.K.Sharma*, J. Phys., **49**, 543, 2019.